Biomaterials 282 (2022) 121390

Contents lists available at ScienceDirect

Biomaterials

journal homepage: www.elsevier.com/locate/biomaterials

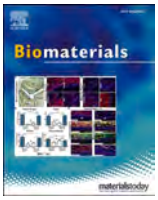

Application of a *Mytilus edulis*-derived promoting calcium absorption peptide in calcium phosphate cements for bone

Zhe Xu [a], Zhixuan Zhu [a], Hui Chen [c], Lingyu Han [a], Pujie Shi [b], Xiufang Dong [d], Di Wu [b], Ming Du [b,**], Tingting Li [a,*]

[a] College of Life Sciences, Key Laboratory of Biotechnology and Bioresources Utilization, Dalian Minzu University, Ministry of Education, Dalian, 116600, China
[b] School of Food Science and Technology, National Engineering Research Center of Seafood, Collaborative Innovation Center of Seafood Deep Processing, Dalian Polytechnic University, Dalian, 116034, China
[c] College of Food Science and Technology, Key Laboratory of Marine Fishery Resources Exploitment & Utilization of Zhejiang Province, Zhejiang University of Technology, Hangzhou, 310014, China
[d] College of Marine Science and Biological Engineering, Qingdao University of Science and Technology, Qingdao, 266042, China

ARTICLE INFO

Keywords:
Mytilus edulis
Peptide
Absorption
Calcium phosphate cements
Bone

ABSTRACT

The IEELEEELEAER peptide (PIE) identified from the protein hydrolysate of *Mytilus edulis* is reported to enhance osteoblast growth and differentiation, which also possesses a superior bone formation ability both *in vitro* and *in vivo*. Moreover, PIE bound to calcium spontaneously at the stoichiometry of 1:1, and there were amino nitrogen and carboxyl oxygen atoms in 2 glutamic acid residues at the calcium-binding sites in the PIE. The PIE–calcium complex facilitated calcium uptake through the Caco-2 cell monolayers. Incorporation of PIE into calcium phosphate cements enhanced calcium ion uptake and proliferation of osteoblasts and inhibit bacteria. This study suggest that calcium phosphate cements supplemented with PIE can serve as a potentially efficient material for bone graft used during spinal surgery.

1. Introduction

Nearly one million cases suffering from skeletal problems need orthopaedic surgery annually. Bone grafts have been extensively used during orthopaedic surgery for promoting bone healing and regeneration [1]. Using calcium phosphate cements (CPCs) to be the bone material for synthesis is investigated from 1980s [2]. CPCs can be used to be the material for bone graft since they are highly biocompatible and osteoconductive, and have similar composition to bone in mineral phase [3].

Many measures are put forward and assessed to promote CPC transformation into new bone, including the increase of porosity or the application of platelet-abundant plasma or water-soluble polymers to be the additives for apatitic CPCs [4–6]. As previously reported, adding mineralised collagen to bone cement improves the bone formation, which is evidenced through the promoted human bone marrow mesenchymal stem cells (BMSCs) to osteoclasts as well as subsequent osteoblasts [7]. In addition, adding collagen into apatitic CPCs was shown to enhance several functional properties; for example, using collagen-containing nanosized hydroxyapatite markedly increases the activity of alkaline phosphatase [8]. Perez and colleagues reported that adding collagen into CPC of liquid phase improves the osteoconductive ability [9]. The solubility of all the calcium phosphate salts of CPC in the body environment is relatively small; the bone cement, which is an ideal bone tissue engineering repair material, is gradually degraded in the body and new bone cells gradually grow into the material. After implantation, the material is gradually absorbed and replaced as the injured bone tissue is repaired and eventually becomes a part of the natural bone tissue. Because of the insufficient degradation properties of such materials, this will hinder the growth of cells and tissues in the body during bone healing. The application of CPC as a repair material for bone tissue engineering is limited. Therefore, it is necessary to improve the crystallinity and biodegradability of CPC and maintain the good fusion and matching degree of CPC and bone. Furthermore, by improving the degradation property of CPC, it can be made a suitable bone tissue engineering repair material.

Numerous recent articles discover that certain bioactive peptides obtained from food proteins form the peptide-calcium complex by

* Corresponding author.
** Corresponding author.
E-mail addresses: duming@dlpu.edu.cn (M. Du), jwltt@dlnu.edu.cn (T. Li).

https://doi.org/10.1016/j.biomaterials.2022.121390
Received 18 December 2021; Accepted 23 January 2022
Available online 1 February 2022

interacting with calcium ions, thereby increasing the calcium uptake, bioavailability and solubility. [10–15]. For such bioactive peptides, their structural characteristics such as composition of amino acid, molecular weight, and specific amino acid groups, are shown to be associated with the ability of metal chelating [11–14,16]. There is an acidic sequence with high polarity in casein phosphopeptides, which contains 3 phosphoserine residues and 2 glutamic acid residues [Ser(P)-Ser (P)-Ser(P)-Glu-Glu], and they account for the calcium chelating sites and affect mineral bioavailability [17]. The use of food-derived polypeptides that bind specifically to their targets is rapidly increasing [18–21].

The aforementioned facts indicated that food-derived peptides with the ability of chelating calcium ions can promote the use of calcium ions in CPC materials. The IEELEEELEAER peptide (PIE) identified from the protein hydrolysate of *Mytilus edulis* has demonstrated superior osteogenic activity in previous studies. In this study, we report that PIE can chelate calcium at a ratio of 1:1 and promote the absorption of calcium ions. With the incorporation of PIE peptide into CPC, the formed CPC material renders the growth and proliferation of osteoblasts easy. The CPC material incorporating the PIE peptide has inhibitory effect on *Escherichia coli* but has no inhibitory effect on *Staphylococcus aureus*. Therefore, this study provides a theoretical basis for promoting new degradable bone healing materials.

2. Materials and methods

2.1. Materials and reagents

MC3T3-E1 and Caco-2 cells were provided by Shanghai Academy of Sciences, China. One calcium-chelating peptide derived from *M. edulis* was discovered through peptidomics. The peptide (purity, 98%) was synthesized via ChinaPeptides Tech Company (Shanghai, China) according to the Fmoc-protected amino acid synthesis method. All the remaining reagents utilized in the present work were analytically pure. β-Calcium phosphate (particle size, < 70 μm) and calcium phosphate monobasic monohydrate were purchased from Aladdin, USA.

PIE–calcium complex was synthesized as per our previously depicted approach after mild modifications [11–14]. Briefly, peptide solution was added into $CaCl_2$ at the 1:10 M ratio under pH 8.0 and 50 °C conditions by 1 h of stirring. Then, the mixed solution was added with ethanol until 90% for complex precipitation. After removing free calcium through 5 min of centrifugation at 12,000*g*, we harvested the precipitate for freeze drying.

2.2. CPC and CPC–PIE discs preparation

Equivalent ground β-calcium phosphate (60.5 mg) was mixed with calcium phosphate monobasic monohydrate (50 mg) into the blender to prepare CPC powders. The CPC discs were prepared through blending CPC powder with water (100 mg of CPC powder with 50 μL water) using a spatula for 30 s. CPC-PIE disc is a mixture of CPC powder, 1% PIE, and 50 μL of water. After placing the paste into the stainless-steel mould for forming the disc of about 0.05-mm thickness and 13.0-mm diameter. Then, the 20 MPa constant pressure was used for 60 s onto the mould by the device. All discs were incubated at 37 °C overnight before removing them from the moulds. CPC/CPC–PIE discs were sterilised through 15 min of soaking within 75% ethanol (mass fraction) and further incubate into α-Minimal essential medium overnight.

The setting time of the cements were tested by Vicat apparatus according to ISO 9597–2008. The final setting time of the cements was defined as the interval that the final setting needle no longer left a visible print on the surface of the pastes. (Ding, Li, Wei, 2018) The test was repeated at least three times for each group. The pastes were transferred into the poly-tetrafluoroethylene mould to form a cylinder with the size of 4.6 mm in diameter and 12 mm in height. The compressive strengths of the cements after setting were tested by electronic universal mechanical testing machine (INSTRON 5982, USA) with a loading rate of 1 mm/min. Each group was repeated at least three times and the average value was calculated.

2.3. Ultraviolet–visible absorption spectroscopy

UV–VIS spectra, detected using a spectrophotometer (PerkinElmer, Salem, MA, USA), were obtained to verify the chelation reaction of PIE with calcium. As described previously [22], PIE was mixed with PBS (pH = 8.0) for obtaining the 20 μg/mL content. Further, 0, 0.5, 1, 1 and 1 μL of 2 M $CaCl_2$ were constantly added to the mixture every 10 min, and wavelengths were scanned between 190 and 400 nm to record the spectra.

2.4. Isothermal titration calorimetry

The affinity ITC calorimeter (TA Instruments Ltd, New Castle, DE, USA) was utilized for ITC assays. Both CaCl2 and peptide were mixed with 50 mM Tris/HCl buffer (pH 8.0), followed by filtration using the 0.22-μm membrane filters as well as 10 min of vacuum degassing prior to titration. After loading $CaCl_2$ to injection syringe to titrate PIE solution, the mixture was added in sample cell. Thereafter, titration was carried out by 30 injections using the automatic sequence, with 2.0 μL $CaCl_2$ solution being titrated to sample cell that contained 350 μL PIE solution each time every 200-s, for the sake of ensuring sufficient equilibration under 25 °C. $CaCl_2$ solution was titrated with Tris-HCl buffer to conduct background titration assay. In every measurement, we completed 3 titrations for ensuring data consistency as well as solution stability. Then, a binding model was used to fit all experimental data. Afterwards, we determined thermodynamic parameters including entropy (ΔS), enthalpy (ΔH), stoichiometry (n) and equilibrium binding constant (K). NanoAnalyze software (TA Instruments) was utilized to process all raw data.

2.5. Fourier-transform infrared spectroscopy

Overall, 2 mg of freeze-dried PIE together with the calcium complex powders was grinded uniformly using KBr (200 mg) in the presence of infrared light, later, the mixture was added onto the Fourier-transform infrared spectrometer (PerkinElmer, Salem, MA) within 4000–800 cm^{-1} region. Each spectrum was obtained under 64 scans and 4 cm^{-1} resolution conditions and analyzed by OMNIC 8.2 software (Thermo Nicolet Co., Madison, WI, USA).

2.6. Circular dichroism

The secondary structure of PIE and PIE–calcium complex was determined by the Jasco J-810 Circular Dichroism Spectroscope (Jasco Co., Tokyo, Japan). All 1 mg/mL samples were analyzed thrice within the 190–260 nm far-UV region.

2.7. TGA

This study conducted TGA using the TGA instrument at nitrogen atmosphere under 30 mL/min (Mettler-Toledo Inc., Switzerland, Zurich). Overall, all 3.0 mg of each sample (PIE and PIE–calcium) were weighed in a crucible to heat from 50 to 600 °C at the 10 °C/min heating rate.

2.8. Transmission electron microscope

TEM (JEM-2100, JEOL, Tokyo, Japan) was utilized to observe PIE–calcium complex morphology. All samples were dispersed into Milli-Q water through ultrasonication. Subsequently, after dropping 1 μL sample solution onto the copper grid, it was dried in air under ambient temperature for TEM characterization.

2.9. MALDI-TOF MS analysis

The PIE–calcium (0.5 mg/mL) was added to 0.1% TFA buffer with 2,5-DHB as matrix. Thereafter, 1 μL of matrix was taken respectively and added into the dried samples. Later, 0.5 μL mixture was placed onto the stainless-steel target plate to dry before conducting the MALDI-TOF MS. Then, we obtained the mass spectra using SmartBeam II laser (355 nm) under the following conditions, acceleration voltage, 20 kv; repetition rate, 200 Hz; reflection mode. 200 laser shots were adopted in each assay. Results were analyzed using FlexAnalysis (version 3.3). We then compared sample molecular peaks with that of the standard (PIE) by using MS/MS at the 50 ppm mass accuracy.

2.10. Molecular docking and optimized PIE–calcium complex structure

In general, the 4-step molecular docking process was adopted to chelate peptides with calcium ions. A new calcium ion model was generated using Discovery Studio 2017 molecular simulation software (Biovia). Second, each peptide sequence was imported into 'Build and Edit Protein' module, followed by optimization of peptide ligand and bond length using Protein Prepare Tool [23]. Then, the Dock Ligands (CDOCKER) approach from DS 2017 software was applied in molecular docking, with calcium ion and complete peptide being the ligand and receptor, respectively. Finally, Receptor-Ligands-Interaction approach from DS 2017 software was adopted to analyse the molecular docking results such as chelating types, distance, and docking energy.

2.11. Calcium transport analysis

Caco-2 cells were obtained from Cell Resource Center of Shanghai Institutes for Biological Sciences, the Chinese Academy of Sciences (Shanghai, China), cultured MEM that contained 20% FBS as well as the 1% penicillin–streptomycin–neomycin antibiotics and incubated under 5% CO_2 and 37 °C conditions. It was constructed the Caco-2 cell monolayer model following our previously depicted approach [15], with the monolayer TEER values $> 500\ \Omega\ cm^2$ being the threshold. PIE at diverse doses (0.5 and 1 mM) or $CaCl_2$ (5 mM) within the 0.5 mL Hank's balanced salt solution (HBSS, pH 7.4) was loaded from the top, followed by 2 h of incubation under 37 °C.

Equivalent samples were collected on basolateral side at specific time points, followed by addition of equivalent HBSS buffer onto basolateral side for maintaining the constant volume. Then, the atomic absorption spectrophotometer (Hitachi Co. Tokyo, Japan) was utilized to measure calcium level.

2.12. Analysis and Characterization of Material Structure

X-ray diffraction (XRD-6000, SHIMADZU, USA) was applied to the characterization and analysis of structures and morphology of the composite cements.

For the purpose of measuring the *in vitro* degradation of cements, the three replicate cements whose thickness and diameter is 0.05-mm and 13.0-mm, respectively were immersed in phosphate buffer saline (PBS, pH = 7.40) with a solid-to-liquid ratio of about 1 g/30 mL. The samples were immersed in a sloshing and constant temperature water path at 37 °C and 70 r/min for 8 days. In this process, the PBS needed refreshing at each test time and every day. After each soaking time, pH test meter (PHS–3C, Shanghai instrument electric science instrument Co. Ltd., China) was employed to collect suspensions whose pH values were subsequently tested and recorded. Besides, 10 h drying at 60 °C was applied to the soaked cements until the weight of the samples remains unchanged. As a control group, the original samples not steeped in PBS were dried directly.

2.13. Osteogenic materials analysis

First of all, we grew MC3T3-E1 cells (2×10^4 cells/well) into CPC material or CPC material with 1% PIE within the 12-well plates. After 48 h, the CPC material that had climbed cells was immersed in PBS thrice, each time for 3 min. The slide was subjected to 15 min of 4% paraformaldehyde fixation, followed by immersion of the glass slide in PBS thrice for 3 min. Subsequently, 5 μg/mL phalloidin staining solution (Beyotime, Shanghai, China) was added, followed by 1 h of incubation under 37 °C, and rinsing using PBS thrice (for 3 min each time). DAPI containing anti-fluorescence quencher (Beyotime, Shanghai, China) was added and incubated for 5 min in dark. DAPI stain was washed using PBS 4 times for 5 min. The samples were observed, and images of IHC slides were examined under a fluorescence microscope (Olympus IX83 microscope, Tokyo, Japan).

MC3T3-E1 cells were seeded in CPC material or in CPC material with 1% PIE within 12-well plates. After 48 h, the material was taken out, washed with PBS, fixed with 2.5% glutaraldehyde, and dehydrated with ethanol gradient. The sample was coated using the gold–palladium alloy for 90 s at 15 mA, SEM images were obtained at the 10 kv accelerating voltage.

MTT assay was used to measure the effect of PIE and PIE-calcium on MC3T3-E1 cell proliferation [24]. In short, cells were cultured in 100 μL of α-MEM and then the resulting cells were inoculated into 96-well culture plates (5×10^4 cells per ml). After 24 h of culture, MC3T3-E1 cells were treated at 37 °C for 24 h, with or without PIE, PIEalcium treatment. Then add 10 μL of MTT (Sigma, USA) solution (5 mg/mL in PBS). After incubating for 4 h, aspirate the supernatant MTT solution, add 150 μL DMSO solution to each well, and use a Microplate Reader (Infinite™ M200, TECAN, Switzerland) to measure the value at 490 nm.

Refer to the instructions of the alkaline phosphatase activity assay kit (Beyotime, Haimen, China) when determining the ALP activity in cells [24].

2.14. Antibacterial assay

E. coli and *S. aureus* were inoculated into LB agar medium, followed by 12 h incubation under 37 °C. A single colony was inoculated into LB broth and placed on a shaker at 37 °C to grow the culture until the OD value reached 0.5. The bacterial solution was diluted to 10^5 CFU/mL. After the addition of 500 μL bacterial solution onto material surface drop by drop, the sample was placed in a 6-well plate to continue the culture. After 12 h, the material was taken out, washed with PBS, fixed with 2.5% glutaraldehyde, and dehydrated with ethanol gradient. The sample was coated using the gold–palladium alloy for 90 s at 15 mA, SEM images were obtained at the 10 kv accelerating voltage.

The *Escherichia coli* and *Staphylococcus aureus* that were activated overnight to OD595 = 0.6 were diluted into fresh LB broth at the ratio of 1:100. PIE was supplemented to the two groups of samples in order to make their final concentrations get to 2000–62.5 μg/mL separately. The same amount of sterile water was added as the control group. Then, 200 μL samples of each group were pipetted into a 96-well plate, which were incubated at 37 °C for 16 h. Finally, the OD value of the samples at 595 nm could be determined.

2.15. Statistical analysis

Data are expressed in a form of mean ± SD. Data significance was analyzed by the Duncan (D)'s post-hoc test using SPSS19.0. $P < 0.05$ stood for statistical significance.

3. Results and discussion

3.1. Calcium chelating ability of PIE peptide

Ultraviolet–visible molecular absorption spectrometry is based on

the molecular valence electron transition of 2 adjacent electronic energy levels. This approach is used to analyse the substantial electronic spectra. For PIE, its UV spectrum was clearly different from that of the PIE–calcium complex (Fig. 1A). The spectrum for PIE displayed a strong absorption peak at approximately 190 nm, and it was the typical peak corresponding to amide bond, carbonyl and carboxyl groups within peptide. As the calcium chloride concentrations increased during chelation, the sample UV intensity increased sequentially, with the sample absorption peak shifting between 1.091 and 1.662 (Fig. 1A) because of carbonyl group within peptide bond transiting from n → π* as well as calcium electron transition [25]. In addition, oxygen atom in carbonyls, along with nitrogen atom within amino group of peptide bond was responsible for alterations in the shift and intensity of the representative absorption peak when calcium ions were bound [26]. Isothermal titration calorimetry (ITC) represents the effective approach to investigate biological binding interactions [27]. The ITC experiment was conducted in the present work for determining thermodynamic parameters related to the interaction of PIE with calcium. Fig. 1B shows raw ITC data regarding PIE peptide solution titration using $CaCl_2$ solution. As a result, ITC data fitted well to the independent binding model, and the reaction stoichiometry (n) was 0.999 ± 0.102, which suggested that PIE contained 1 binding site for calcium. Similarly, the study by Cui et al. came to consistent results, which revealed the presence of 1 binding site for calcium within peptide (EDLAALEK) from sea cucumber ovum [28]. Collectively, the band shifts indicated that PIE binds to the calcium ion and thus forms a compact PIE–calcium chelate.

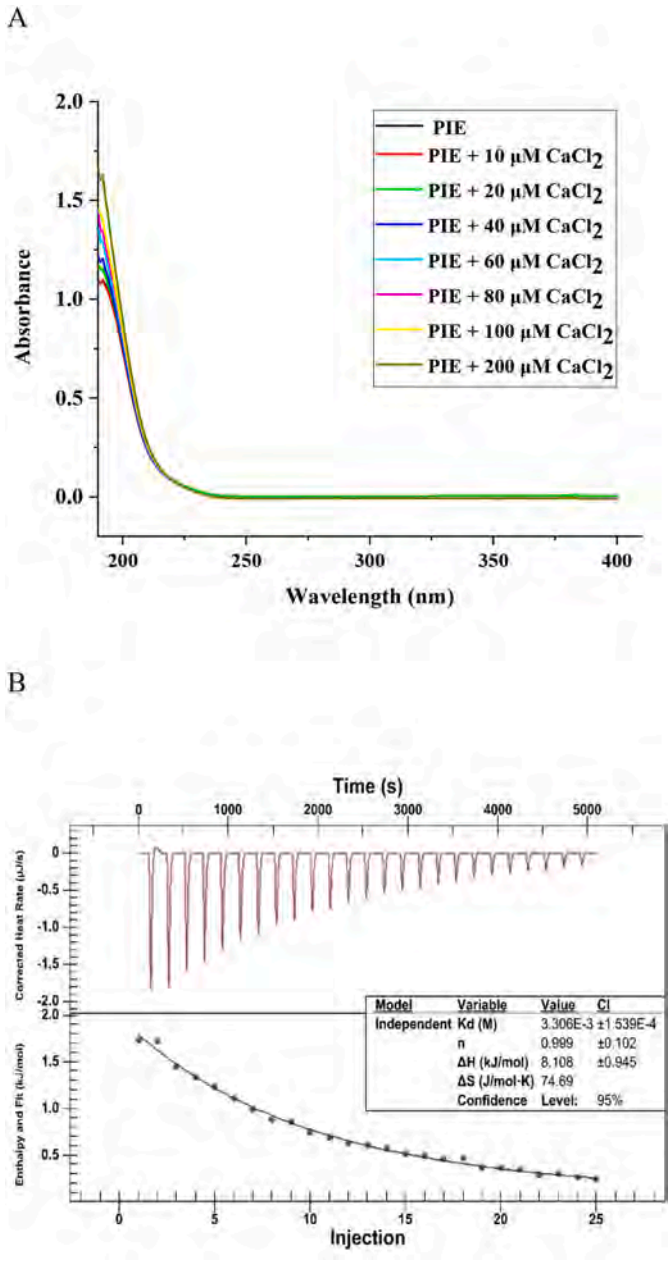

Fig. 1. Peptide IEELEEELEAER (PIE) and calcium ion chelation (A) UV spectra of PIE with different $CaCl_2$ concentrations over the wavelength range from 190 to 400 nm (B) The raw ITC data obtained from continuous injection of 2.0 μL $CaCl_2$ solution to PIE solution. Titration plot derived from the integrated heats of binding of the raw ITC data.

3.2. Calcium binding studies

Variations in the Fourier-transform infrared spectroscopic (FTIR) spectra for PIE were seen after calcium ions bound to amino acid residues of PIE [29]. Fig. 2A displays FTIR spectra for PIE along with the formed calcium complex. Those characteristic absorption frequencies for the carboxyl functional groups on PIE were 1195.21 cm^{-1} (C–O stretching vibration) as well as 1656.76 cm^{-1} (C═O stretching vibration). After the combination of carboxyl functional groups with calcium ions, the corresponding absorption frequencies were found to shift to 1314.80 cm^{-1} and 1622.54 cm^{-1}, respectively. This result is consistent with those of a study by Hou [30]. The shift in absorption frequencies may be caused by the interaction between the carboxyl functional group of PIE and calcium ions.

Through metal coordination, peptides' behaviour is frequently accompanied with alterations of peptide secondary structure. Circular dichroism (CD) spectroscopy has been the efficient approach to investigate changes in protein or peptide secondary structural conformation [31]. For evaluating the Ca^{2+} role in PIE secondary structure, we recorded CD (Fig. 2B). PIE within water shows a great negative CD peak (around 196 nm), which indicates the representative conformation of secondary structures [11–14]. Following binding of calcium with PIE, one significantly decreased negative peak occurred at approximately 196 nm. The α-helix and β-turn conformation reduced, while β-sheet conformation elevated after the binding of calcium ion with PIE. Such structural alterations were associated with calcium ion binding to PIE affinity site, thus producing PIE–calcium nanocomposite.

Heated PIE and PIE–calcium was investigated using the thermogravimetric analysis (TGA) (Fig. 2C). 2 wt loss processes were seen in thermogravimetric curves for each sample. The first one was seen at less than 120 °C, and it was associated with water evaporation [32]. The second stage (150 °C-450 °C) showed fast weight loss and was associated with structural damage [33]. PIE peptide began to degrade at 117 °C, although the degradation speed was relatively slow; the degradation speed increased at 236 °C. In contrast, PIE–calcium began to degrade at 258 °C, and the degradation rate increased at 312 °C. This result indicated that PIE forms a new structure after chelating with calcium ions. The high peak temperature and a slow degradation rate indicated that the PIE–calcium complex possesses a high thermal stability. The transmission electron microscopic (TEM) images for PIE–calcium complex revealed spherical nanoparticles with relative uniformity (Fig. 2D).

3.3. Molecular docking of PIE–calcium complex

The sequence in PIE with calcium-chelating ability was identified using matrix-assisted laser desorption ionisation-time of flight mass spectrometry (MALDI-TOF MS). Molecular weight of PIE was 1488.57, and the *m/z* of PIE measured by MALDI-TOF MS was 1488.632; a peak with *m/z* of 1528.655 was observed, as shown in Fig. 3. The difference between the two *m/z* was 40.023, which is approximately the molecular weight of calcium. This finding indicated that some PIE chelates calcium to form the PIE–calcium complex.

Molecular docking has been extensively adopted for predicting the

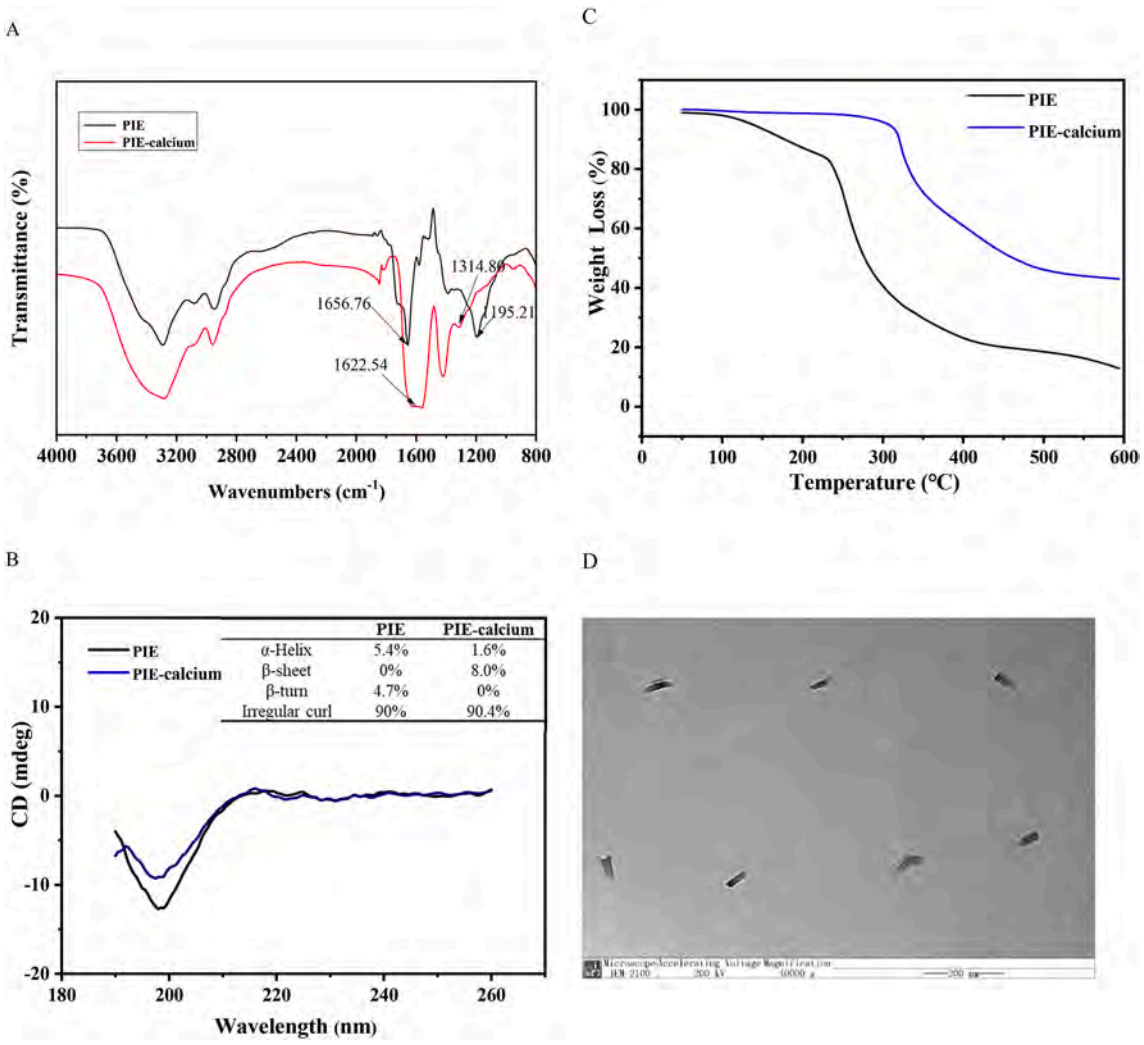

Fig. 2. Conformational and morphological analysis. (A) Fourier transform infrared spectroscopy spectra of the PIE and PIE-calcium complex in the regions from 4000 to 800 cm^{-1}. (B) Far-UV circular dichroism spectroscopy of the PIE and PIE-calcium complex over the range of 190–260 nm, insets show their secondary structure relative content of α-helix, β-sheet, β-turn and random coil. (C) TG curves of PIE and heated complexes of PIE-calcium. (D) TEM imaging of the PIE-calcium complex.

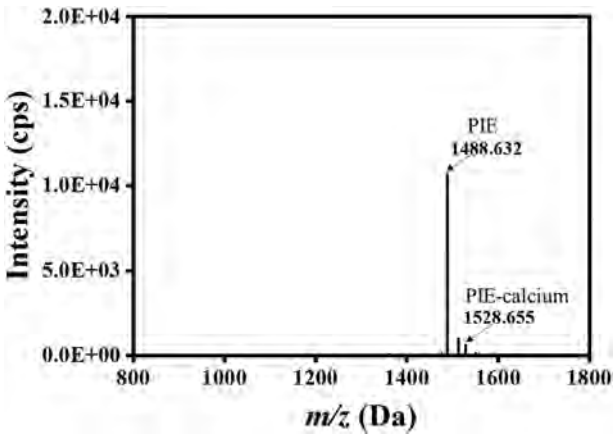

Fig. 3. PIE-calcium complex identified using MALDI-TOF MS.

associations of ligands with receptors through assessing chelating sites, docking energies, as well as additional data related to the interaction [24,34]. Therefore, molecular docking was applied in analyzing the potential calcium-chelating mechanism in PIE. As shown in Fig. 4A, calcium ions were docked with PIE as the center. Glutamate was found to be the chelation site, as shown in Fig. 4B. This result was consistent with that of a study by Li and colleagues, which indicated that peptides containing acidic amino acids (glutamic acid) are main chelation sites. [35]. As shown in Fig. 4B, the docking type is a metal acceptor, which indicates the interaction between calcium ions and carbonyl groups. Such finding conformed to that of a prior report indicating that calcium ions can form complexes with negatively charged carboxylate groups [30]. The results were similarly to those obtained from FTIR.

3.4. Calcium absorption studies

This study adopted the Caco-2 cell monolayer model for monitoring calcium ion absorption triggered by PIE. After addition of different concentrations of PIE and $CaCl_2$ from the top, samples were collected on the bottom for 30, 60, 90, and 120 min. As shown in Fig. 5, PIE could promote the transport and absorption of calcium ions. The higher the PIE concentration, the more significant is the effect. These data indicated that PIE promoted calcium uptake through the Caco-2 cell monolayer. In a study, PIE peptides were shown to be relatively stable during absorption and to reach the blood circulation for metabolism [36]. Therefore, PIE could promote not only the transport of calcium ions but also the use of calcium ions.

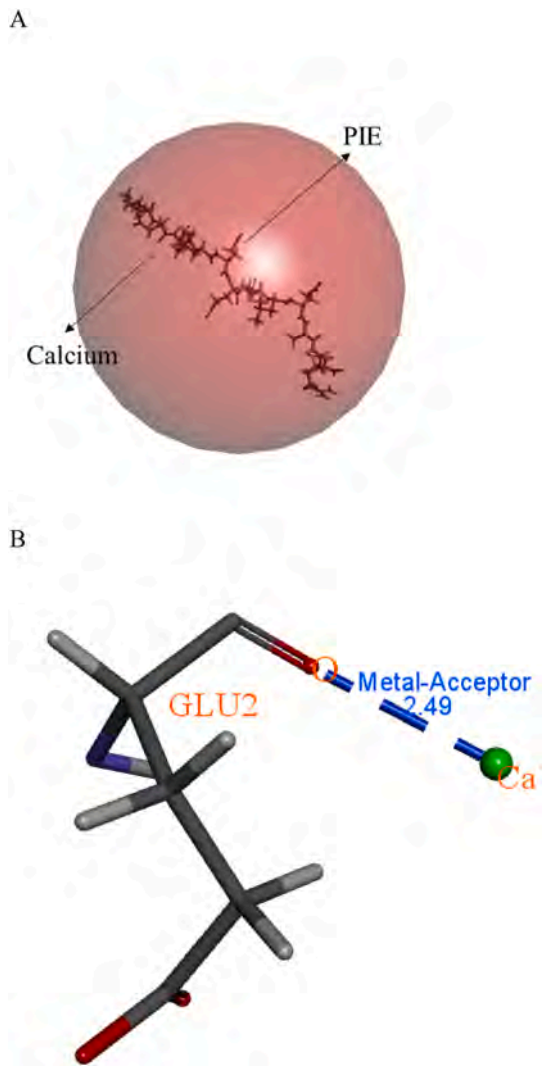

Fig. 4. Molecular docking and optimized structure of the PIE-calcium complex. (A) 3D structure of PIE-calcium complex as a surface image, generated by the surface menu of Discovery Studio 2017 software. (B) Interaction between GLU2 in PIE with calcium.

3.5. PIE in CPC promotes osteoblast proliferation

Cell culture toxicity assay has been the globally accepted approach to initially screen the biocompatibility of biomaterials because its rapidness, reproducibility, sensitivity and cost-effectiveness compared with animal testing. Therefore, cell culture *in vitro* was used for evaluating the new cement formulation biocompatibility that contained PIE peptide (CPC–PIE) (Fig. 6A). MC3T3-El cells, the osteoblast-like cells in mice [37], were grow on the CPC–PIE discs or CPC discs, followed by overnight culture and observation under a microscope for the evaluation of adhesion and morphology. Because the opacity of cement discs, fluorescence microscope or SEM was adopted to view cells that grew on cement disc surface.

In fluorescence assays, we used phalloidin and DAPI to stain cells. DAPI stained the cell nuclei blue, whereas phalloidin stained the cell membrane red (Fig. 6B). Adherence of live cells was observed, which kept the normal, polygonal shape [38] after seeding on CPC–PIE or CPC discs. Thereafter, panels were qualitatively examined, which suggested that cells adhering to CPC–PIE discs showed a higher density than that of cells adhered to CPC discs. This result indicated the great cell adhering ability to CPC–PIE and CPC. Additionally, CPC–PIE was found show low or no toxicity to cells compared with CPC. CPC–PIE was more conducive

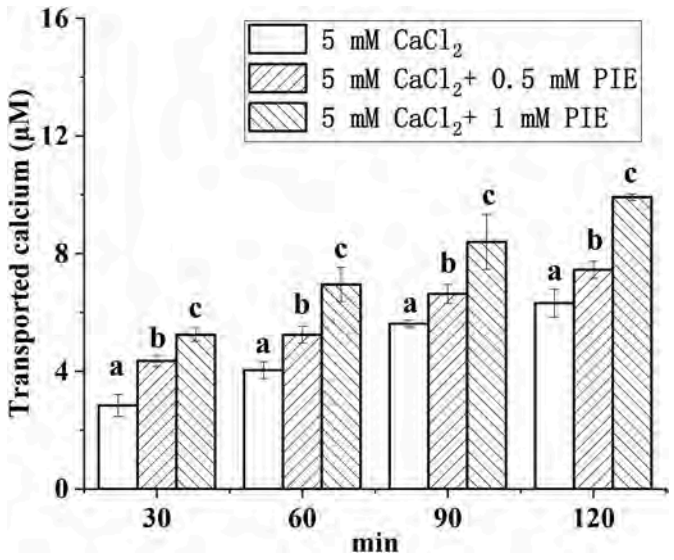

Fig. 5. Calcium transport studies. Different concentrations of the PIE (0.5 and 1 mM) or 5 mM $CaCl_2$ in 0.5 mL of Hank's balanced salt solution (HBSS, pH 7.4) were added to the apical side, and incubated at 37 °C for 2 h. Aliquots were extracted from the basolateral side at 30, 60, 90, and 120 min, and an equal volume of HBSS buffer was added to the basolateral side to keep the volume constant. Calcium contents were determined by using an atomic absorption spectrophotometer. Different letters indicate significant difference among the groups at the given time point ($p < 0.05$).

to the proliferation of osteoblasts than CPC. After overnight culture, high resolution images were acquired by the SEM. Cells adhered and spread onto CPC–PIE discs more efficiently than on CPC discs (Fig. 6B). This finding is consistent with a that of a study which reported that PIE peptide enhanced osteoblast growth and differentiation [39]. Therefore, CPC–PIE could promote the growth of osteoblasts on its surface.

3.6. Antibacterial effect of PIE in CPC

E. coli and *S. aureus* can affect the healing effect of materials on wounds. [40]. The *in vitro* antibacterial capacity of PIE in CPC was evaluated. After PIE treatment, the number of *E. coli* cells were slightly wrinkled (Fig. 6C). The morphology of the *E. coli* cell membrane is wrinkled, indicating that PIE can enhance the inhibitory effect of CPC materials on *E. coli* (Fig. 6C). However, PIE does not have a good antibacterial effect on *S. aureus*. In Fig. 6C, the peptide PIE did not produce a zone of inhibition against *E. coli* and *S. aureus* but it was found that PIE had a slight inhibitory effect on *E. coli* through OD measurement, but it had no obvious effect on *S. aureus*. This is consistent with the results of SEM performance.

3.7. Effect of PIE on the properties of CPC materials

The XRD patterns of PIE, PIE-caladium, CPC and CPC-PIE are demonstrated in Fig. 7A. The main diffraction peaks of CPC are mainly attributed to the reaction products $Ca_3(PO_4)_2$ and $CaHPO_4$. The new diffraction peaks appearing in CPC-PIE are compared with CPC and PIE-calcium. After PIE is added, it is chelated with the calcium in CPC. And the crystallinity of CPC did not change significantly after PIE was added. It shows that CPC has an initial setting time of 22.08 min and a final setting time of 26.46 min in Fig. 7B. With the addition of PIE, the initial setting time increased to 34.7 min, and the final setting time increased to 38.78 min. On this basis, it can be inferred that the coagulation time of CPC can be prolonged after PIE is added. The setting of compressive strength of CPC and CPC-PIE is presented in Fig. 7B. It is apparent that increasing PIE exerts no effect on the strength of compressed cement. Fig. 7C exhibits the weight loss periods of CPC and CPC-PIE after they

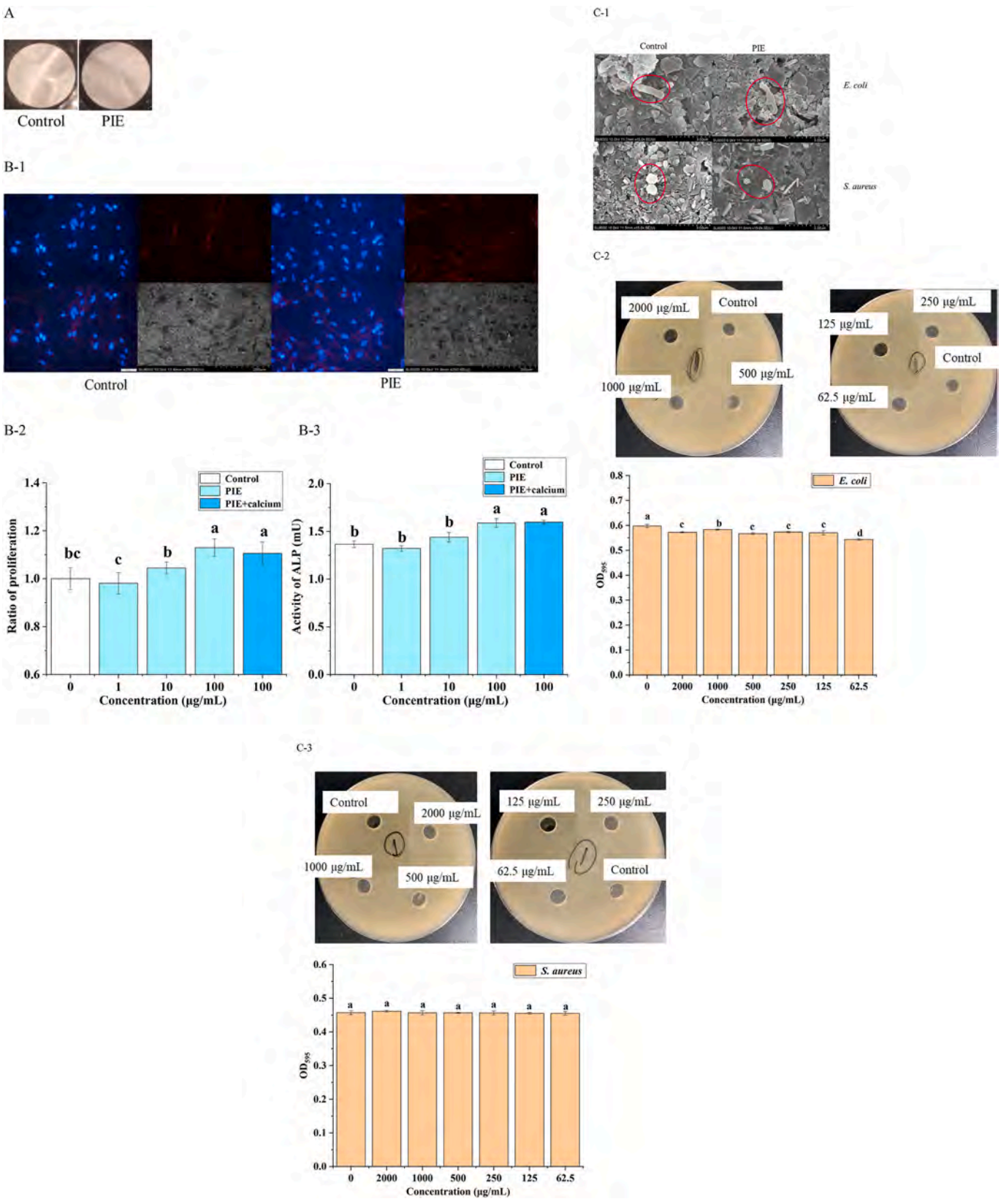

Fig. 6. The MC3T3-E1 cells and morphologies in materials. (A)Photos of CPC materials or CPC material with 1% PIE. (B-1) Fluorescence images and SEM images of the MC3T3-E1 cells in CPC material or CPC material with 1% PIE. (B-2, B-3) The proliferation and ALP activity of the peptide PIE on MC3TE-E1. (C-1) Morphologies of E. *coli* and S. *aureus* placed in CPC material or CPC material with 1% PIE. (C-2, C-3) The antibacterial effect of peptide PIE on *Escherichia coli* and *Staphylococcus aureus*. Different letters indicate significant difference among the groups at the given time point ($p < 0.05$).

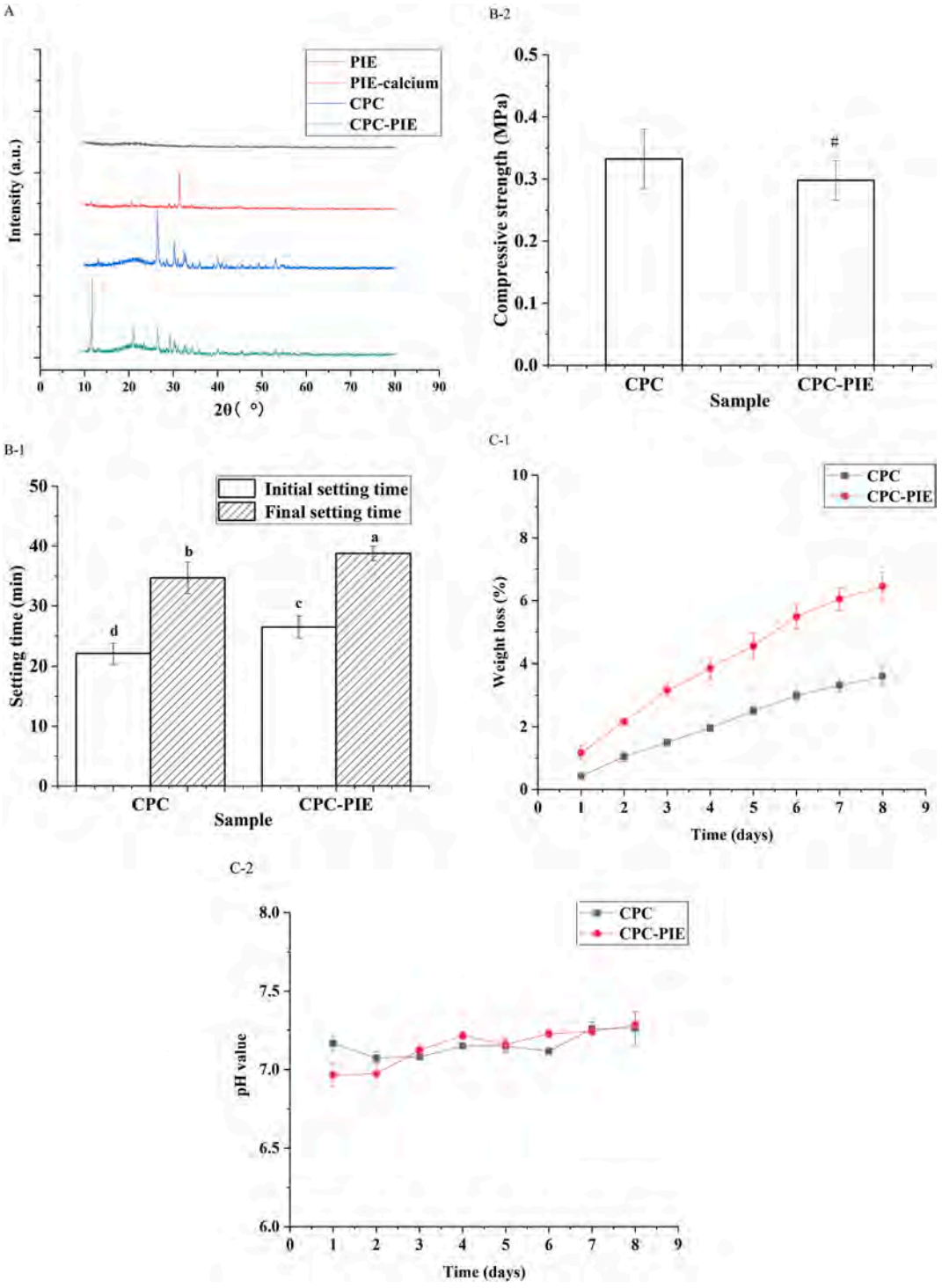

Fig. 7. Analysis and Characterization of Material Structure. (A) The XRD patterns of the PIE, PIE-calcium, CPC and CPC-PIE. (B) The setting times and the compressive strength of the CPC and CPC-PIE. (C) The weight loss and pH value of the composite cements after soaking in PBS for different times. Different letters indicate significant difference among the groups at the given time point ($p < 0.05$). "#" indicates that there is no significant difference from the control group.

are soaked in PBS for different times. All cements degrade at a slow speed. Compared with the degradation of CPC, the degradation rate of CPC with PIE is faster, which is consistent with the previous conclusion that PIE can promote calcium absorption. And both CPC and CPC-PIE remained at 6.9–7.3 for 8 days as shown in Fig. 7C.

4. Conclusion

In summary, the new calcium-binding peptide obtained in *M. edulis* was studied. PIE peptide could enhance calcium ion absorption in Caco-2 model. PIE peptide also bound to calcium at the stoichiometry of 1:1; besides, there were carboxyl oxygen atoms from 2 glutamic acid residues in the PIE peptide in binding site for calcium. Incorporation of PIE into CPC could promote the absorption of calcium ions and proliferation of osteoblasts and inhibit bacteria. Therefore, CPC–PIE could serve as a suitable potentially material for bone graft adopted during spinal surgery.

Declaration of competing interest

All authors declare that they have no conflicts of interest.

Acknowledgements

This work was supported by the National Key R&D Program of China (2018YFD0400601) and the open fund of Key Laboratory of Marine Fishery Resources Exploitment & Utilization of Zhejiang Province (SL2021004).

References

[1] C. Laurencin, Y. Khan, S.F. El-Amin, Bone graft substitutes, J. E. r. o. m. d 3 (1) (2006) 49–57.
[2] R. LeGeros, Calcium phosphate materials in restorative dentistry: a review, J. A. i. d. r 2 (1) (1988) 164–180.
[3] J. Barralet, T. Gaunt, A. Wright, I.R. Gibson, J. Knowles, Effect of porosity reduction by compaction on compressive strength and microstructure of calcium phosphate cement, J. J. o. B. M. R. A. O. J. o. T. S. f. B., Jpn. Soc. Biomater. Biomater. T. A. S. f., Biomater. t. K. S. f. 63 (1) (2002) 1–9.
[4] A. Almirall, G. Larrecq, J. Delgado, S. Martınez, J. Planell, M.J.B. Ginebra, Fabrication of low temperature macroporous hydroxyapatite scaffolds by foaming and hydrolysis of an α-TCP paste, Biomaterials 25 (17) (2004) 3671–3680.
[5] J.-C. Chen, C.-L. Ko, C.-J. Shih, Y.-C. Tien, W.-C. Chen, Calcium phosphate bone cement with 10 wt% platelet-rich plasma *in vitro* and *in vivo*, J. J. o. d 40 (2) (2012) 114–122.
[6] L. Sun, H.H. Xu, S. Takagi, L.C. Chow, Fast setting calcium phosphate cement-chitosan composite: mechanical properties and dissolution rates, J. J. o. b. a 21 (3) (2007) 299–315.
[7] J. Wu, S. Xu, Z. Qiu, P. Liu, H. Liu, X. Yu, F.-Z. Cui, Z.R. Chunhua, Comparison of human mesenchymal stem cells proliferation and differentiation on poly (methyl methacrylate) bone cements with and without mineralized collagen incorporation, J. J. o. b. a 30 (6) (2016) 722–731.
[8] R. Perez, G. Altankov, E. Jorge-Herrero, M. Ginebra, Micro-and nanostructured hydroxyapatite–collagen microcarriers for bone tissue-engineering applications, J. J. o. t. e., Med. r. 7 (5) (2013) 353–361.
[9] R.A. Perez, M.-P. Ginebra, Injectable collagen/α-tricalcium phosphate cement: collagen–mineral phase interactions and cell response, J. J. o. M. S. M. i. M 24 (2) (2013) 381–393.
[10] H. Chen, P. Shi, Z. Xu, F. Fan, Z. Wang, M. Du, Oral Administration of Oyster Peptide Prevents Bone Loss in Ovariectomized Mice, J. e. 1 (4) (2020) 298–309.
[11] N. Sun, P. Cui, Z. Jin, H. Wu, Y. Wang, S. Lin, Contributions of molecular size, charge distribution, and specific amino acids to the iron-binding capacity of sea cucumber (Stichopus japonicus) ovum hydrolysates, J. F. c 230 (2017) 627–636.
[12] N. Sun, P. Cui, D. Li, Z. Jin, S. Zhang, S. Lin, Formation of crystalline nanoparticles by iron binding to pentapeptide (Asp-His-Thr-Lys-Glu) from egg white hydrolysates, J F., Funct. 8 (9) (2017) 3297–3305.
[13] N. Sun, P. Cui, S. Lin, C. Yu, Y. Tang, Y. Wei, Y. Xiong, H. Wu, Characterization of sea cucumber (Stichopus japonicus) ovum hydrolysates: calcium chelation, solubility and absorption into intestinal epithelial cells, J. J. o. t. S. o. F., Agric. 97 (13) (2017) 4604–4611.
[14] N. Sun, Z. Jin, D. Li, H. Yin, S. Lin, An exploration of the calcium-binding mode of egg white peptide, Asp-His-Thr-Lys-Glu, and *in vitro* calcium absorption studies of peptide–calcium complex, J. J. o. a., Chem. f. 65 (44) (2017) 9782–9789.
[15] Z. Xu, F. Fan, H. Chen, P. Shi, D. Zhu, M. Yang, Z. Wang, H.R. Ei-Seedi, M. Du, Absorption and transport of a Mytilus edulis-derived peptide with the function of preventing osteoporosis, J. F., Funct. 12 (5) (2021) 2102–2111.
[16] L. Guo, P.A. Harnedy, B. Li, H. Hou, Z. Zhang, X. Zhao, R. FitzGerald, Food protein-derived chelating peptides: Biofunctional ingredients for dietary mineral bioavailability enhancement, J. J. T. i. F. S., Technol. 37 (2) (2014) 92–105.
[17] M.J. García-Nebot, R. Barberá, A. Alegría, Iron and zinc bioavailability in Caco-2 cells: influence of case in ophosphopeptides, J. F. c 138 (2–3) (2013) 1298–1303.
[18] X. Cai, J. Lin, S. Wang, Novel peptide with specific calcium-binding capacity from Schizochytrium sp. protein hydrolysates and calcium bioavailability in Caco-2 cells, J. M. d 15 (1) (2017) 3.
[19] T. Hou, C. Wang, Z. Ma, W. Shi, L. Weiwei, H. He, Desalted duck egg white peptides: promotion of calcium uptake and structure characterization, J. J. o. a., Chem. f. 63 (37) (2015) 8170–8176.
[20] P. Minkiewicz, J. Dziuba, A. Iwaniak, M. Dziuba, M. Darewicz, BIOPEP database and other programs for processing bioactive peptide sequences, J. J. o. A. I 91 (4) (2008) 965–980.
[21] L. Sánchez-Rivera, D. Martínez-Maqueda, E. Cruz-Huerta, B. Miralles, I. Recio, Peptidomics for discovery, bioavailability and monitoring of dairy bioactive peptides, J. F. R. I 63 (2014) 170–181.
[22] J. Lin, X. Cai, M. Tang, S. Wang, Preparation and evaluation of the chelating nanocomposite fabricated with marine algae Schizochytrium sp. protein hydrolysate and calcium, J. J. o. a., Chem. f. 63 (44) (2015) 9704–9714.
[23] C. Vats, J.K. Dhanjal, S. Goyal, N. Bharadvaja, A. Grover, Computational design of novel flavonoid analogues as potential AChE inhibitors: analysis using group-based QSAR, molecular docking and molecular dynamics simulations, J. S. C. 26 (2) (2015) 467–476.
[24] Z. Xu, H. Chen, Z. Wang, F. Fan, P. Shi, M. Tu, M. Du, Isolation and characterization of peptides from *mytilus edulis* with osteogenic activity in mouse MC3T3-E1 preosteoblast cells, J. J. o. a., Chem. f 67 (5) (2019) 1572–1584.
[25] Y. Yu, D. Fan, Characterization of the complex of human-like collagen with calcium, J. B. t. e. r 145 (1) (2012) 33–38.
[26] C.A. Blindauer, I. Harvey, K.E. Bunyan, A.J. Stewart, D. Sleep, D.J. Harrison, S. Berezenko, P. Sadler, Structure, properties, and engineering of the major zinc binding site on human albumin, J. J. J. o. B. C 284 (34) (2009) 23116–23124.
[27] K. Zhou, S. Yang, G. Zhao, Y. Ning, C. Xu, Self-assembly of the sodium salts of fatty acids into limpid hydrogels through non-covalent interactions with peptides, J. R. A 5 (76) (2015) 61719–61724.
[28] P. Cui, S. Lin, W. Han, P. Jiang, B. Zhu, N. Sun, Calcium delivery system assembled by a nanostructured peptide derived from the sea cucumber ovum, J. J. o. a., Chem. f. 67 (44) (2019) 12283–12292.
[29] F.-R. Liu, L. Wang, R. Wang, Z.-X. Chen, Calcium-binding capacity of wheat germ protein hydrolysate and characterization of peptide–calcium complex, J. J. o. a., Chem. f. 61 (31) (2013) 7537–7544.
[30] H. Hou, S. Wang, X. Zhu, Q. Li, Y. Fan, D. Cheng, B. Li, A novel calcium-binding peptide from Antarctic krill protein hydrolysates and identification of binding sites of calcium-peptide complex, J. F. c 243 (2018) 389–395.
[31] S. Zhang, R. Liang, Y. Zhao, S. Zhang, S. Lin, Immunomodulatory activity improvement of pine nut peptides by a pulsed electric field and their structure–activity relationships, J. J. o. a., Chem. f. 67 (13) (2019) 3796–3810.
[32] Y. Tian, Y. Li, X. Xu, Z. Jin, Starch retrogradation studied by thermogravimetric analysis (TGA), J. C. P 84 (3) (2011) 1165–1168.
[33] L. Zhu, G. Wu, L. Cheng, H. Zhang, L. Wang, H. Qian, X. Qi, Investigation on molecular and morphology changes of protein and starch in rice kernel during cooking, J. F. c 316 (2020) 126262.
[34] M. Tu, C. Wang, C. Chen, R. Zhang, H. Liu, W. Lu, L. Jiang, M. Du, Identification of a novel ACE-inhibitory peptide from casein and evaluation of the inhibitory mechanisms, J. F. c 256 (2018) 98–104.
[35] Z. Zhang, F. Zhou, X. Liu, M. Zhao, Particulate nanocomposite from oyster (*Crassostrea rivularis*) hydrolysates via zinc chelation improves zinc solubility and peptide activity, J. F. c 258 (2018) 269–277.
[36] Z. Xu, H. Chen, F. Fan, P. Shi, S. Cheng, M. Tu, H.R. Ei-Seedi, M.J. Du, Pharmacokinetics and transport of an osteogenic dodecapeptide, J. o. A., Chem. F. 68 (37) (2020) 9961–9967.
[37] H. Sudo, H.-A. Kodama, Y. Amagai, S. Yamamoto, S.J.T. Kasai, *In Vitro* differentiation and calcification in a new clonal osteogenic cell line derived from newborn mouse calvaria, J. o. c. b 96 (1) (1983) 191–198.
[38] C.G. Simon Jr., C.A. Khatri, S.A. Wight, F.W. Wang, Preliminary report on the biocompatibility of a moldable, resorbable, composite bone graft consisting of calcium phosphate cement and poly (lactide-co-glycolide) microspheres, J. J. o. o. r 20 (3) (2002) 473–482.
[39] Z. Xu, H. Chen, F. Fan, P. Shi, M. Tu, S. Cheng, Z. Wang, M. Du, Bone formation activity of an osteogenic dodecapeptide from blue mussels (*Mytilus edulis*), J. F., Funct. 10 (9) (2019) 5616–5625.
[40] Y. Liu, Y. Xiao, Y. Cao, Z. Guo, F. Li, L. Wang, Construction of chitosan-based hydrogel incorporated with antimonene nanosheets for rapid capture and elimination of bacteria, J. A. F. M 30 (35) (2020) 2003196.